

1 **Air pollution reductions caused by the COVID-19 lockdown open up a way to preserve**
2 **the Himalayan Glaciers**

3
4 Suvarna Fadnavis^{1*}, Bernd Heinold², T. P Sabin¹, Anne Kubin², Katty Huang³, Alexandru
5 Rap⁴, and Rolf Müller⁵

6 ¹Indian Institute of Tropical Meteorology, Centre for climate change research, Ministry of
7 Earth Sciences, India

8 ²Leibniz-Institut für Troposphärenforschung, Leipzig, Germany,

9 ³Urban Climate, Risk & Health, UCL, London, United Kingdom

10 ⁴School of Earth and Environment, University of Leeds, Leeds, UK,

11 ⁵Forschungszentrum Jülich GmbH, IEK-7, Jülich, Germany,

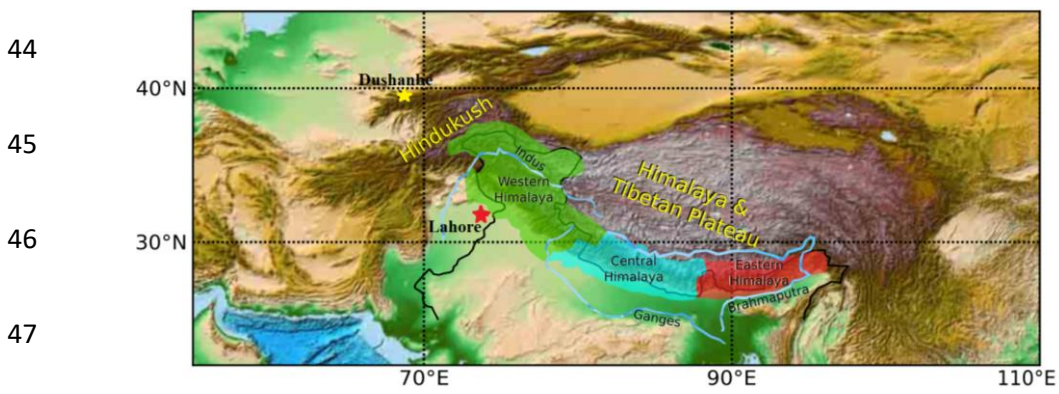
12 Corresponding author email: suvarna@tropmet.res.in

13 Abstract

14 The rapid melting of glaciers in the Hindu Kush Himalayas (HKH) during recent decades poses
15 an alarming threat to water security for larger parts of Asia. If this melting persists, the entire
16 Himalayan glaciers are estimated to disappear by end of the 21st century. Here, we assess the
17 influence of the spring 2020 COVID-19 lockdown on the HKH, demonstrating the potential
18 benefits of a strict emission reduction roadmap. Chemistry-climate model simulations,
19 supported by satellite and ground measurements, show that lower levels of gas and aerosol
20 pollution during lockdown led to changes in meteorology, and to a reduction in black carbon
21 in snow (2-14%) and thus in snow melting (10-40%). This caused increases in snow cover (6-
22 12%) and mass (2-20%) and a decrease in runoff (5-55%) over the HKH and Tibetan Plateau,
23 ultimately leading to an enhanced snow-equivalent-water (2–55%). We emphasize the
24 necessity for immediate anthropogenic pollution reductions to address the hydro-climatic threat
25 to billions of people in South Asia.

27 **1. Introduction**

28 The Hindu Kush Himalayan (HKH) mountains and Tibetan plateau is the largest snow-cladded
29 region outside the Poles (Fig. 1). This region is also referred to as High Mountain Asia,
30 although that includes the Tien Shan and some other northern ranges. The HKH meltwater
31 feeds rivers in India and China that drive the agriculture, hydropower generation, and economy
32 of these countries (Hussain et al., 2019; Sabin et al., 2020; Lee et al. 2021a). The Himalayan
33 snowmelt in spring provides ~50% of the annual freshwater to ~4 billion people of South Asia
34 and East Asia (Sarangi et al 2019, Sabin et al., 2020). Rapid Himalayan snowmelt caused a
35 loss of ~40 % of the Himalayan glacier area compared to the Little Ice Age, 400 to 700 years
36 ago, i.e. ~0.92 to 1.38 mm sea-level equivalent (Lee et al., 2021b). The snow mass over the
37 Himalayas has generally decreased during the last 30 years (except for a few Karakoram
38 glaciers that show an increasing trend in snow mass) (Hussain et al., 2019. The alarming rate
39 of snow melting of 0.02 to 0.6 cm °C⁻¹ day⁻¹ raised concerns about the sustainability of water
40 supply (Tiwari et al., 2015) and loss of glaciers in the region (Hussain et al., 2019, Lee et al.,
41 2021b). Model simulations for extreme scenarios show that Himalaya snow melting could
42 cause the glaciers to disappear by the end of the 21st century (Cruz et al. 2007, Hock et al.,
43 2019).



48 **Figure 1:** Map of the Hindu Kush Himalayas region with the Western (70 - 80° E, 30° - 35° N),
49 Central (80° - 87° E, 28° - 30° N), and Eastern Himalayas (88° - 95° E, 26° - 30° N). A yellow
50 and red star indicates the location of the AERONET sun photometer stations Dushanbe
51 (68.858° E, 38.553 ° N) and Lahore (74.264° E, 31.480° N), respectively.

52 The accelerated thinning of Himalayan glaciers is attributed to climate change causing
53 shifts in air temperature and precipitation, as well as the atmospheric distribution and
54 deposition of light-absorbing particles i.e., dust and black carbon (BC) (IPCC Climate Change
55 2013, Krishnan et al., 2019). Among the aforementioned factors, snow darkening due to the
56 deposition of absorbing aerosols is an integral component of Himalayan snowmelt and runoff
57 (Lau et al., 2010). The snow-melting efficacy of BC is higher than that of greenhouse gases
58 (Qian et al., 2011; Nair et al. 2013; Ma et al., 2019; Sarangi et al., 2019). The increasing energy
59 demand of the densely populated South Asian region has increased the emission of greenhouse
60 gases and BC aerosol in the last few decades (Fadnavis et al., 2017, Krishnan et al., 2020),
61 leading to enhanced darkening and snow melting (Usha et al., 2021).

62

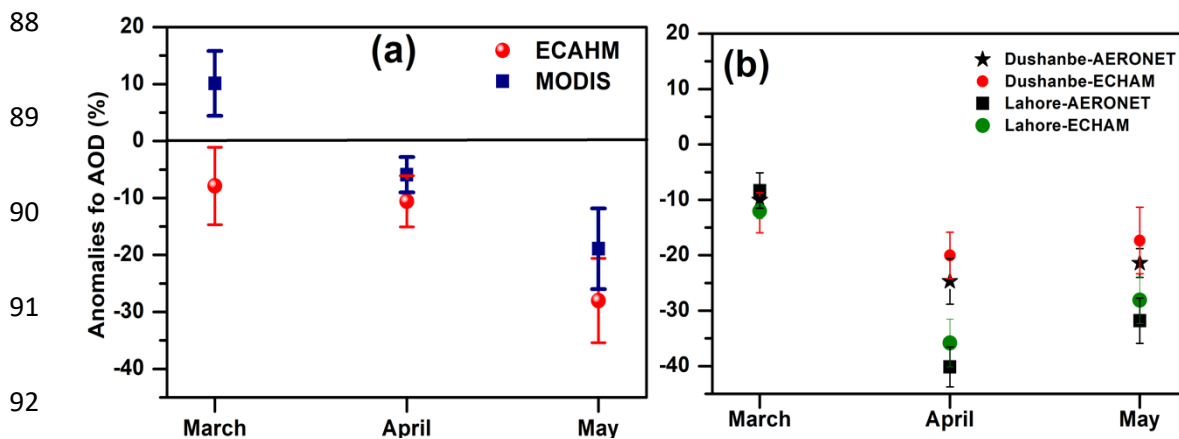
63 The economic slowdown caused by the COVID-19 pandemic measures led to a drastic
64 reduction in public and freight transportation, industrial emissions, and energy use (Fadnavis
65 et al., 2021a). This resulted in a substantial decline in emissions of several atmospheric
66 pollutants including greenhouse gases and black carbon aerosol (Forster et al. 2020; Kanniah
67 et al., 2020; Le Quéré et al 2020), and potentially reduced deposition of dark aerosols on snow
68 and ice (Bair et al., 2021). Remote sensing approaches show cleaner snow with ~30% less
69 light-absorbing impurities in snow during the lockdown period over Asia between March and
70 May 2020 (Bair et al 2021). This led to decreased snowmelt by 25 – 70 mm in 2020 compared
71 to the last 20-year mean for March-May over Western Himalayas due to decreased radiative
72 forcing induced by BC and dust deposition on snow/ice surfaces and related changes in snow
73 absorption and surface albedo (Bair et al., 2021). Bair et al. (2021) also found that 6.6 km⁻³ of
74 melt water stayed in the Indus Basin. Gauge and reservoir data for this part of the world,
75 however, are not freely available. Impacts of reduced levels of air pollution on changes in the
76 snow mass, surface water runoff, and water reservoir over the HKH are not reported hitherto.

77 Here, we provide a detailed analysis of the impact of reduced pollution over HKH and Tibetan
 78 plateau region during the COVID-19 lockdown period between March and May 2020. We used
 79 global simulations with the chemistry-climate model ECHAM6-HAMMOZ (Schultz et al.,
 80 2018, Tegen et al., 2019), updated with an improved BC-in-snow parameterization (Huang
 81 2018), in order to contrast the 2020 COVID-19 (COVID) with the typical, unchanged (control,
 82 CTL) air pollution conditions. The COVID simulations are performed using a COVID-19
 83 emission inventory where emissions are reduced based on Google and Apple mobility data
 84 (Forster et al., 2020; details in section S1).

85

86 2 Results

87 2.1 Reduction of airborne aerosols and in-snow BC concentration over the Himalayas



93 **Figure 2:** (a) Changes in monthly mean AOD (%) during March - May 2020 from MODIS in
 94 comparison to mean of 2001-2019 and ECHAM-HAMMOZ (COVID minus CTL) averaged
 95 over the Hindu Kush Himalayas (HKH) and Tibetan Plateau region (75° - 95° E, 30° - 35° N),
 96 (b) same as (a) but for AOD from AERONET observations and ECHAM-HAMMOZ model
 97 results at Dushanbe (68.858° E, 38.553° N, climatology 2010-2019) and Lahore (74.264° E,
 98 31.480° N, climatology 2006-2019). Vertical bars in Fig (a)-(b) indicate the standard deviation
 99 within ten members of model simulations, and within monthly mean anomalies from MODIS
 100 for years 2001-2019.

101

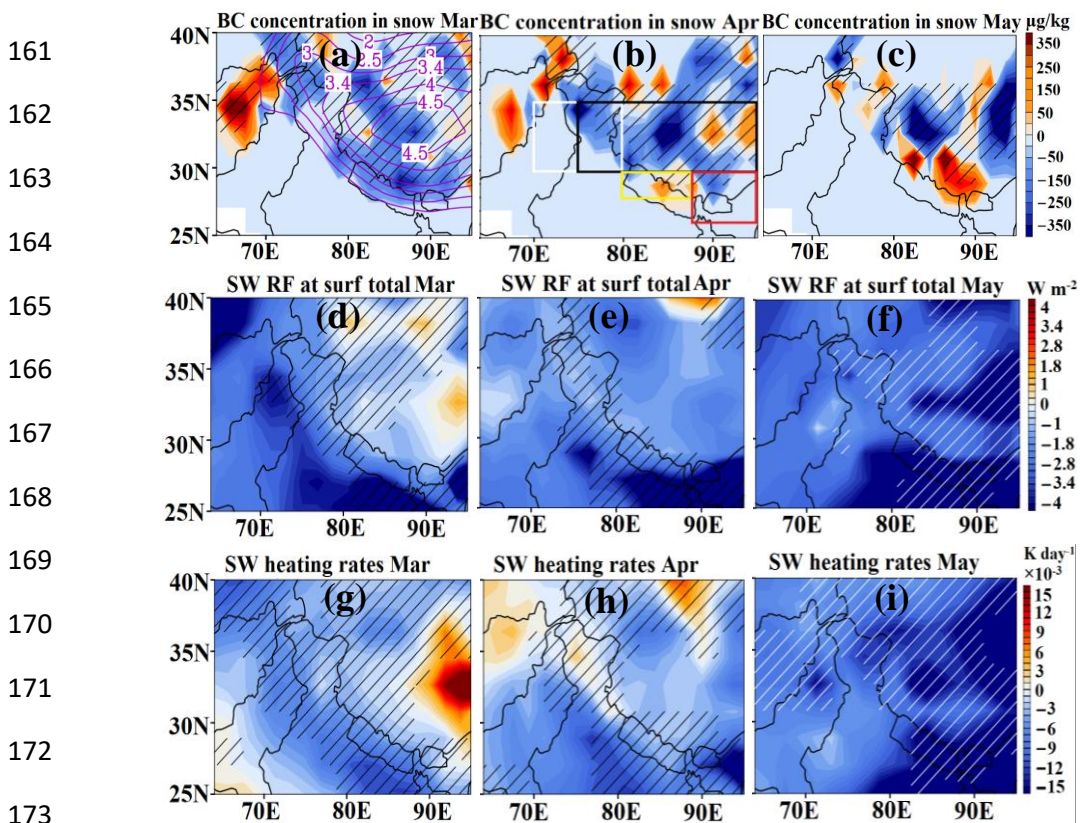
102 The COVID-19 lockdown restrictions in spring 2020 decreased the anthropogenic
103 aerosol amounts over the HKH ranges (Western, Central, and Eastern Himalayas), and the
104 Tibetan Plateau region. The ECHAM6-HAMMOZ model simulations show that COVID
105 lockdown resulted in a cleaner atmosphere during March - May 2020 over the HKH ranges and
106 Tibetan Plateau region. There is a reduced level of Aerosol Optical Depth (AOD) over the
107 region throughout spring 2020 by -8.1 ± 6.2 % in March, -10.2 ± 4.7 % in April, -27 ± 6.9 % in
108 May compared to the CTL (non COVID) simulation (Fig. 2a). This is supported by NASA's
109 Moderate Resolution Imaging Spectroradiometer (MODIS) measurements also showing a
110 reduction in AOD in April (-5.6 ± 3.3 %) and May (-18.8 ± 7.2 %) 2020 compared to the mean
111 over the last 20 years (Fig. 2a). Thus, both model simulations and MODIS AOD show a
112 reduction in aerosol pollution in April - May 2020. For March 2020, MODIS measurements
113 show AOD enhancement by 10.2 ± 4.8 %, which is due to increased dustiness over the HKH
114 region (see section S2 for a detailed discussion). AOD measurements at two Aerosol Robotic
115 Network (AERONET) sun photometer stations in Dushanbe (68.858° E, 38.553° N)
116 and Lahore (74.264° E, 31.480° N) show an AOD reduction in agreement with our model
117 simulations (Fig. 2b). There are differences among MODIS, AERONET and the model. The
118 changes in AOD during COVID compared to no-COVID period is less in the model than the
119 MODIS observations by 4.2 - 9.8 % and higher than the AERONET observations by 1.8 - 4.2
120 %. These differences are due to the fact that the simulated AOD change is in response to the
121 reduction of anthropogenic aerosols and associated circulation responses, while MODIS and
122 AERONET measurements show the effect of all atmospheric processes. Also, note that the
123 MODIS AOD values are spatial averages representative for a relatively large area while the
124 AERONET values are point measurements. Importantly, changes in simulated AOD in 2020
125 fall within the standard deviation of satellite and ground-based measurements indicating
126 reliability of our simulations (except for March 2020 with respect to MODIS). Our model

127 simulations also show a reduction in BC burden by 15 - 55% (Fig. S1a), and sulfate burden by
128 22 - 24 % over the HKH and Tibetan Plateau regions in spring 2020 (Fig. S1b). Interestingly,
129 dust burden also shows a reduction over these regions (Fig. S1c, Fig. S2a-c), except over central
130 Himalaya in March and April 2020. The lower dust load is related to the interactive change in
131 atmospheric dynamics in the model, which also leads to changes in the wet and dry deposition
132 rates of dust (Fig. S2d-i) (details in section S2). A drop in BC is also observed in Aerosol
133 Radiative Forcing Over India Network (ARFINET) ground-based measurements over the Indo-
134 Gangetic Plain (> 50 %), north-eastern India (>30%), Himalaya regions (16 - 60%), and Tibet
135 (70%) during spring 2020 (Gogoi et al., 2021; Liu et al., 2021). A similar impact of the
136 reduction of energy consumptions on decrease in AOD during the COVID-19 lockdown period,
137 i.e., in spring 2020 compared to the 2010-2019 climatology is also seen over South and East
138 Asia (40 %) and the Indo-Gangetic Plain (IGP) by 30 – 40 % in satellite measurements
139 (Fadnavis et al., 2021a; Srivastava et al., 2021; Pandey et al., 2021; Shafeeque et al., 2021).

140

141 The reduction in anthropogenic air pollution leads widely to a reduction in BC
142 concentration in the snow of approximately 25 - 350 $\mu\text{g kg}^{-1}$ (by 12 – 35 %) during spring 2020
143 (Fig. 3a-c) that reduce the snow darkening effect by embedded aerosol impurities. At the most
144 this amounts to about a 1.6% increase in visible snow albedo. Sporadically, however, the BC-
145 in snow concentrations have also increased in some areas of the Hindukush, Eastern Himalayas
146 and Kunlun Mountains. There are many factors at play that may lead to an increase in BC
147 concentration in snow in some locations. For instance, this includes increases in deposition of
148 BC following shifts in the atmospheric circulation (Fig.S3), accumulation of BC on surface
149 snow following partial snowmelt and minimal fresh snowfall, and less frequent occurrences of
150 complete snowmelt which would otherwise remove all accumulated BC in snow. Our
151 simulations reveal that the decrease in BC-in snow concentration and the overall reduction in

152 atmospheric pollution, as well as associated radiative effects, have decreased the shortwave
 153 radiative forcing at the surface by $0.2 - 2 \text{ W m}^{-2}$ in March – May 2020 (Fig. 3 d-f), leading to
 154 a decrease in tropospheric heating by solar radiation of 0.001 to 0.015 K day^{-1} (Fig. 3 g-i). The
 155 reduced anthropogenic BC over the HKH and Tibetan Plateau region resulted in less absorption
 156 and re-emission of longwave radiation and, as a consequence, there is a reduction in longwave
 157 radiative forcing in the atmosphere leading to a lower atmospheric heating (Fig. S4). Therefore,
 158 the reduction of anthropogenic sulfate, OC, BC burden, combined with lower atmospheric
 159 loadings of PM2.5 and PM10, as well as BC in snow resulted in decreased heating of the
 160 snowpack and tropospheric column.



174 **Figure 3:** Spatial distribution of anomalies (COVID minus CTL) of BC concentration in snow
 175 ($\mu\text{g kg}^{-1}$) for (a) March, (b) April, and (c) May 2020; (d-f) shortwave radiative forcing (W m^{-2})
 176 at the surface and (e-g) tropospheric heating rates (K day^{-1}) due to changes in BC
 177 concentration in snow (COVID minus CTL). Hatched areas indicate the 95%-significance
 178 level. Contours in panel (a) indicate topography in km. Boxes in panel (b) indicate boundaries
 179 of Western Himalayas (WH, white), Central Himalayas (CH, yellow), Eastern Himalayas (EH,
 180 red) and Tibetan Plateau (black).

181 **2.2 Impacts on snow melting, surface water runoff, and snow cover**

182 Further we show that the decrease in aerosol pollution reduced the snow melting in
183 spring 2020 by 0.2 to 2.5 mm day⁻¹ corresponding to 10 – 50 % (Fig. 4 a-c). The amount of
184 reduction of snow melting is pronounced over the western Himalayas in May. As a result of a
185 reduction in snowmelt, surface water runoff has been drastically reduced by 2-4 mm –ay⁻¹ (5 -
186 55 %) (Fig. 4 d-f). The reduction in the runoff is most pronounced in May over the entire
187 Himalayas and central Tibetan Plateau region. Estimates from remote sensing measurements
188 also show the reduction of runoff by 6.5 km³ of melted water in the Indus River Basin (Bair et
189 al. 2020). In the past, studies have shown that elevated levels of light-absorbing aerosols
190 (elemental carbon: 13 to 75 ng g⁻¹ and dust: 32 to 217 µg g⁻¹) can contribute to about 3 to
191 10 mm day⁻¹ of snowmelt over western Himalayas (Thind et al. 2019). A sensitivity analysis
192 by (Santra et al., 2019) using a glacier mass balance model shows that BC-induced snow albedo
193 reduction leads to an increase in annual runoff of 4 – 18%. In contrast to impacts of rising
194 anthropogenic emissions during the past decades, emission reductions during the 2020
195 COVID-19 lockdown period caused a brighter snow albedo and therefore an enhanced surface
196 reflection with albedo increases of 0.2 – 0.5 (see Fig. 4g-i), leading to less atmospheric heating
197 as well as associated reduced snowmelt and surface water runoff in spring 2020.

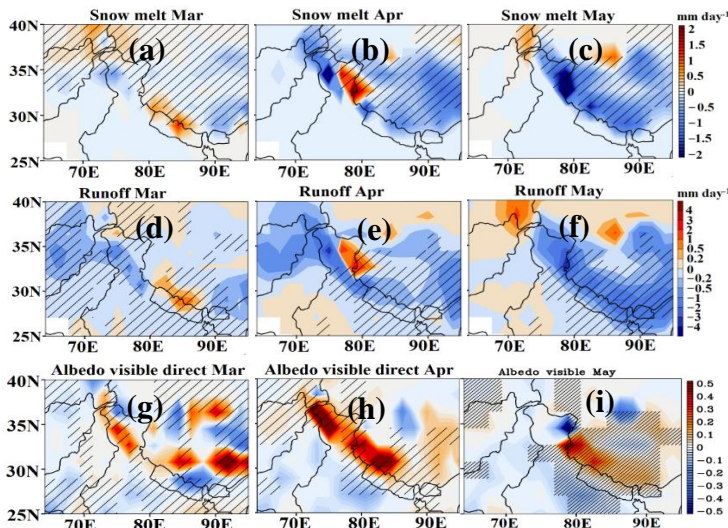
198

199

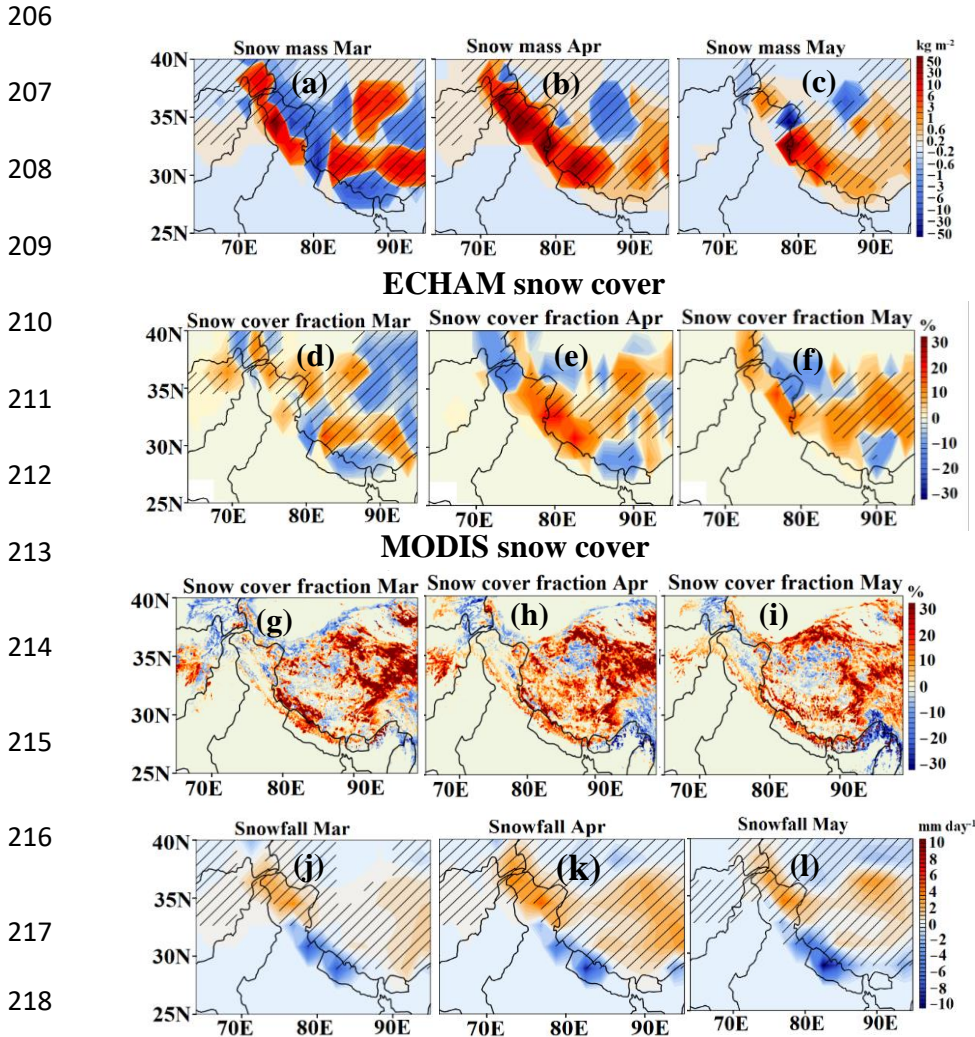
200

201

202



203 **Figure 4:** Spatial distribution of anomalies of (a-c) snow melt (mm day^{-1}), (d-f) surface water
 204 runoff (mm day^{-1}) for March to May 2020 (COVID minus CTL) and (g-i) surface albedo mean
 205 in the visible. Hatched areas indicate the 95%-significance level.



219 **Figure 5:** Monthly mean anomalies (COVID minus CTL) for March to May 2020 of (a-c) the
 220 snow mass (kg m^{-2}), (d-f) snow cover fraction (%) as modelled by ECHAM6-HAMMOZ as
 221 well as (g-i) snow cover fraction from MODIS satellite measurements (%) with respect to the
 222 climatological average 2000-2019, and, (j-l) snowfall as modelled by ECHAM6-HAMMOZ.
 223 Hatched areas indicate the 95%-significance level.

224

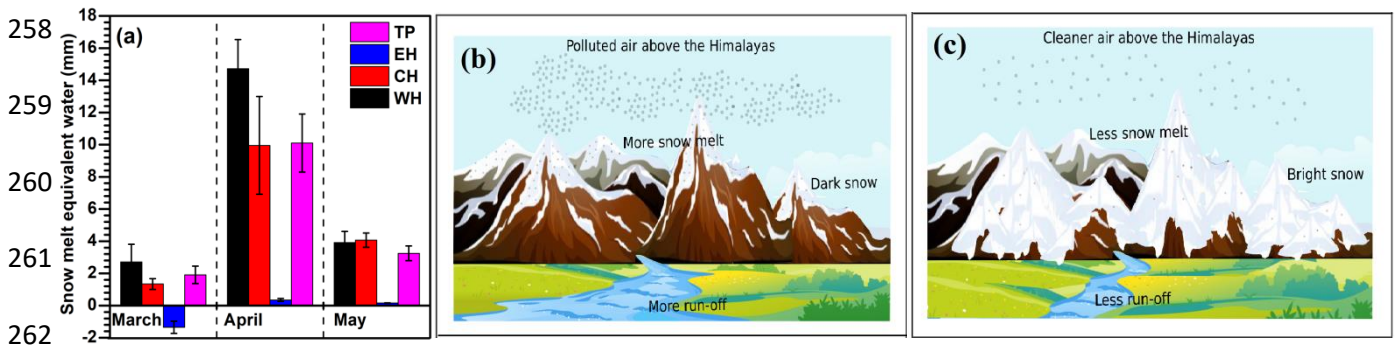
225 Our simulations also indicate that these changes lead to an increase in snow mass of
 226 $0.2\text{-}50 \text{ kg m}^{-2}$, i.e. 10-40% (Fig. 5a-c) and snow cover fraction of 2-30% during spring 2020
 227 (Fig. 5d-f). MODIS measurements also show a remarkable agreement with the model
 228 simulations (especially during April - May 2020), with increased snow cover of about 15-30%

229 over the parts of Western Himalayas and Central Himalayas and the Tibetan Plateau region
230 and decreased by 5-12 % over parts of North-East Himalayas especially in April and May 2020
231 (Fig. 5 g-i). However, there are also some differences in terms of exact regions of snow cover
232 enhancement or reduction respectively, since the MODIS observations include the influence of
233 real-time meteorology, while meteorology in the model ensemble include internal variability
234 and do not replicate the exact conditions observed by MODIS. Our model simulations show
235 that air pollution reductions in the COVID-19 lockdown period and associated changes in
236 radiative forcing caused changes in the tropospheric circulation and thermodynamics (see
237 Fadnavis et al., 2020 for a detailed analysis). These changes in meteorology have increased
238 snowfall by 2-5 mm day⁻¹ (3-20 %) over the Western Himalayas and Tibetan Plateau region
239 (Fig. 5 j-l). The increase in snowfall over these regions will contribute to enhancement in snow
240 mass and snow cover (Fig. 5 a-f) and albedo (Fig. 4 g-i). In a few areas, however, this also
241 contributes to a more efficient BC deposition on snow, as described above (Fig. 3). This BC
242 enrichment in snow at a few places, however, has no influence on the fact that overall the
243 COVID-19 measures reduced the BC-in snow concentration and thus increased the visible
244 snow albedo (see Fig. 4g-i).

245

246 Himalaya snow is the largest source of freshwater for South Asia (Bolch et al., 2012).
247 The impact of reduced pollution on the surface water content in the Himalayas from our model
248 simulations is illustrated in Fig. 6a. The snow mass enhancement led to increase the snow
249 equivalent water by 2 to 14.7 mm (2.5 to 55 %). The western Himalayas show the highest
250 increase in snow equivalent water by 14.7 mm (55 %) followed by the Tibetan Plateau by 12
251 mm (by 22 %) and central Himalayas by 10 mm (by 18%) in April while the Eastern Himalayas
252 show a decrease in March (-1.3 mm; 10 %) and small enhancement in April by 1.1mm (2.3 %) and
253 and May 2020 by 1.3 mm (2.7%) due to pollution reduction. Thus, human induced pollution

254 reduction during the COVID-19 lockdown benefitted the HKH in many ways. A schematic
 255 shows the COVID-19 lockdown-induced effects in Figs. 6b-c: increased snow surface
 256 reflectivity, reduced snowmelt and surface water runoff, as well as enhanced water content in
 257 the reservoir and snow.



263 **Figure 6:** (a) Change in water content (mm) of the Himalayan surface reservoirs (COVID
 264 minus CTL) from March to May 2020 over the Western Himalayas (WH), Central Himalayas
 265 (CH), Eastern Himalayas (EH) and Tibetan Plateau (TP). Vertical bars indicate the standard
 266 deviation within ten members of model simulations. Schematic illustrating the impacts of (b)
 267 air pollution on snow darkening in the Himalayas and surface water runoff for the usual
 268 polluted case and (c) the impacts of reduced pollution on snow brightening in the Himalayas
 269 and reduced surface water runoff, as observed during the 2020 COVID-19 lockdown period.

270

271 **3. Summary and conclusions:** A rising trend in Asian air pollution and associated
 272 climate change over the last few decades has had a detrimental impact on snow melting over
 273 the Hindu Kush Himalayas (HKH) and Tibetan Plateau region (Wester et al., 2019). Black
 274 carbon from increasing emissions of biomass burning, industrial and domestic combustion and
 275 transport is deposited on snow, reducing its albedo (i.e. darkening) (Bolch et al., 2019). A snow
 276 darkening effect along with pollution reduction, compounded with other climate change
 277 effects, accelerates the melting of snow and the disappearance of ice cover over the HKH and
 278 Tibetan Plateau region at an extraordinary rate (Usha et al., 2021). The drop in anthropogenic
 279 air pollution emissions, e.g. from energy production, during the COVID-19 lockdown period
 280 in spring 2020 reduced air pollutant levels worldwide (Forster et al., 2020). Our model

281 simulations indicate that the associated reduction in anthropogenic aerosols and greenhouse
282 gases in spring 2020 has benefited the HKH snow reservoirs. It caused an enhancement in the
283 snow cover fraction by 6 - 12 % and snow mass by 2 - 20 %, corresponding to a decrease in
284 snow melting by 10 - 40% and surface water runoff by 0.2 - 3 mm day⁻¹. As a consequence,
285 the water content of the reservoir increased considerably by 4 to 59 %.

286 Our findings highlight that out of the two processes causing a retreat of Himalayan glaciers:
287 (1) a slow response to global climate change and (2) a fast response to local air pollution
288 (especially black carbon), a policy action on the latter is more likely to be within reach of
289 possible policy action on a shorter-term time scale and a more regional spatial scale. Even if
290 we stopped CO₂ emissions immediately, temperatures would not start decreasing. Our findings
291 confirm the importance of reducing short-lived climate forcers (black carbon) and their
292 complementary role to CO₂ mitigation (Rogelj et al., 2014). Reduction of air pollution to levels
293 similar with those recorded during the 2020 COVID-19 lockdown period, could safeguard
294 HKH glaciers, which are otherwise under the threat to disappear by the end of the 21st century.
295 Since 2000 Himalayan glaciers have been losing nearly half a meter of ice per year (Wester et
296 al., 2019). Our estimates indicate that air pollution reduction during COVID 19 lockdown in
297 spring 2020 caused a reduction in snow melt by 0.5 to 1.5 mm day⁻¹, indicating large benefits
298 to HKH glaciers. Even if global warming is kept below 1.5°C, one third of the glaciers in the
299 HKH region and more than half of those in the Eastern Himalaya will likely be lost by the end
300 of this century (Bolch et al., 2019). The speedily retreating glaciers and the snowpack loss are
301 already posing a threat to domestic sustainable water resources for billions of people in Asia
302 (Wood et al., 2021). However, if new economically and technically feasible policies would
303 reduce emissions of air pollutants (in particular black carbon) to at least lockdown period
304 levels, snowmelt could be reduced by 10 – 50%. Such policies will therefore bring substantial
305 benefits for sustained water supply, agriculture, and ecosystems in large parts of Asia.

307 **Section S1: Methods:**

308 S1.1 Observational data

309 We used monthly snow cover fraction from NASA's Moderate Resolution Imaging
310 Spectroradiometer (MODIS) satellite product on a $0.5 \times 0.5^\circ$ resolution (version 6, level 3; Hall
311 et al., 2006) for the years 2000 – 2020 (<https://nsidc.org/data/MOD10CM/versions/6>). For
312 aerosol information we used monthly mean satellite AOD at $1 \times 1^\circ$ resolution from the MODIS
313 Terra level-3 dark target and deep blue retrievals at 550 nm wavelength for 2001-2020
314 (<https://giovanni.gsfc.nasa.gov>). Uncertainty in MODIS AOD data over snow are documented
315 by Huang et al (2020). We also used ground-based sun photometer observations of AOD from
316 the Aerosol Robotic Network (AERONET) (Martonchik et al., 2004) at the stations Dushanbe
317 (68.858° E, 38.553° N) for the period 2010-2020 and Lahore (74.264° E, 31.480° N) for the
318 period 2006 – 2020, situated in HKH region (<https://aeronet.gsfc.nasa.gov>).

319

320 **S1.2 The ECHAM6-HAMMOZ model description and Experimental set-up**

321 We performed 10-member ensemble experiments using the state-of-the-art aerosol-
322 chemistry-climate model ECHAM6-HAMMOZ (version echam6.3-ham2.3-moz1.0; Schultz et
323 al., 2018, Tegen et al., 2019). The model comprises the atmospheric general circulation model
324 ECHAM6 (Stevens et al., 2013), the atmospheric chemistry module MOZ (Schultz et al, 2018),
325 and the Hamburg Aerosol Model (HAM; Stier et al., 2005; Zhang et al., 2012). The HAM
326 component predicts the nucleation, growth, evolution, and sinks of sulphate (SO_4^{2-}), black
327 carbon (BC), particulate organic matter (POM), sea salt (SS), and mineral dust (DU) aerosols.
328 Seven log-normal modes describe the size distribution of the aerosol population with a
329 prescribed variance in the aerosol module. The MOZ submodule describes the trace gas
330 chemistry from the troposphere to the lower thermosphere. The chemical mechanism includes

331 the O_x, NO_x, HO_x, ClO_x and BrO_x chemical families, along with CH₄ and its degradation
332 products. Several primary non-methane hydrocarbons (NMHCs) and related oxygenated
333 organic compounds are also described. It contains 108 species, 71 photolytic processes, 218
334 gas-phase reactions and 18 heterogeneous reactions with aerosol (Schultz et al., 2018). Details
335 of emissions (anthropogenic, biomass burning, biogenic, fossil fuel etc.) and model
336 parametrisation and other details are reported in the past Fadnavis et al. (2017, 2019a,b, 2021b).
337 Anthropogenic and biomass burning emissions of sulphate, and black carbon (BC) and organic
338 carbon (OC) are based on the AEROCOM-ACCMIP-II emission inventory for year 2020
339 (Lamarque et al., 2010; Textor et al., 2006). Additional consideration for the reduction of snow
340 albedo due to BC in snow is implemented but extended for the MOZ module. Snow albedo
341 reduction is calculated by considering the concentration of BC in the top layer of surface snow.
342 Influxes of BC in snow include below-cloud and in-cloud wet scavenging, as well as dry
343 deposition and sedimentation. Snowmelt and glacier runoff remove the in-snow BC at a
344 reduced efficiency, leading to enhanced concentration, while fresh and pristine snowfall leads
345 to reductions in BC concentration.

346

347 The model simulations were performed at T63 horizontal resolution ($1.875^\circ \times 1.875^\circ$) with 47
348 levels in the vertical from the surface to 0.01 hPa (corresponding to approx. 80 km), and with
349 a time step of 20 minutes. To understand the effect of the COVID-19 restrictions on snow over
350 Himalayas and Tibetan plateau region we conducted a control (CTL) and a COVID-19
351 (COVID) simulation. We adopted an ensemble approach (with 10 ensemble members) for the
352 above two experiments. Ten spin-up simulations were performed from 1 to 31 December 2019
353 to generate stabilised initial fields for the 10 ensemble members. Emissions were the same in
354 each of the 10 members during the spin-up period. Control simulations were extended with the
355 same setup until 1 June 2020. While for the COVID simulations (10 ensemble members each),

356 the anthropogenic emission of all gases and aerosols were changed since 1 January 2020
357 according to Google and Apple mobility data as in Forster et al. (2020). The COVID-19
358 emissions were prepared by deriving scaling factors between the input4MIPS SSP245 baseline
359 and the version5 of the Forster et al. (2020) 2-year blip scenario, separately for each species
360 and each grid point (see Fig. S5a). Subsequently, these scaling factors have been applied to the
361 AeroCom-II ACCMIP emissions. This ensures consistency of the drop in emissions
362 independent of the absolute emission values in the AeroCom-II ACCMIP and the input4MIPS
363 SSP245 data sets. The global mean emission changes in carbon monoxide (CO, 2-24%), black
364 carbon (BC, 3-23%), organic carbon (OC, 2-17%), sulfur dioxide (SO₂, 3-23%), nitrogen o
365 xides (NO_x, 2-30%), methane (CH₄, 2-5%), and ammonia (NH₃, 0-3%) during the period
366 January to 1 July 2020 (COVID - CTL) are in agreement with previous studies Forster et al.
367 (2020) and Le Quéré et al., (2020) (Fig. S5b). Our model experiments follow the CovidMIP
368 protocol (Jones et al., 2021). The COVID and CTL simulations ended on 1 June 2020. To
369 investigate the effects of COVID-19 emissions in spring (i.e., since 1 March 2020), we
370 analysed the difference between COVID and CTL simulations for the spring season in 2020.
371 The same dust parametrisation was employed in the CTL and COVID simulations.

372 A limitation of our simulation is the relatively coarse spatial resolution in the ECHAM6-
373 HAMMOZ model (1.875°x1.875°). Other studies used a finer spatially resolved regional
374 model; for example Sarangi et al. (2020) use a 12 x 12 km (~ 0.10°) grid in the regional WRF-
375 Chem-SNICAR model over the same region. In our model grid of 1.875°, many of the
376 Himalayan sub ranges are smaller than a pixel, and, hence, the topographic influences, which
377 are substantial in the mountains are limited. One effect may be that snowfall and snow on the
378 ground are underestimated (e.g., Liu et al., 2022). The coarse grid size can impact the anomalies
379 found here as the changes in snow mass are small, at most +16 mm, and the bias in the likely
380 underestimated snow mass may change between the control and COVID simulations. Biases

381 are, however, the same in the control and COVID simulations and, thus, their effects will be
382 diluted when we compute the anomalies.

383 **Section S2: Comparison of AOD over Western, Central, Eastern Himalayas and Tibetan** 384 **Plateau regions**

385 We elaborate on the comparison of MODIS AOD with our model simulations over
386 Western, Central, Eastern Himalayas and Tibetan Plateau regions (Fig. S6). Both MODIS and
387 the model show a reduction in AOD during spring 2020 over the aforementioned regions of
388 HKH. The estimated differences in AOD during March to May 2020 vary between 0.8 – 11%
389 over Western and Central Himalayas, and 8 – 16% over Eastern Himalayas. Over the Tibetan
390 plateau region, in contrast to the model simulations, MODIS shows an enhancement (2 – 16 %)
391 in AOD (Fig. S6). This may be due to dust aerosols, which are transported during spring from
392 western Asia and locally, generating dust piles over the Tibetan Plateau (Fadnavis et al., 2017,
393 2021a). The simulated dust aerosol concentration in spring 2020 over the Tibetan Plateau
394 region is smaller in the COVID than in the non-COVID (i.e. CTL) situation (Fig. S1c). The
395 changes in simulated dust are a response to meteorology differences between the COVID and
396 CTL simulations (Fig. S7).

397

398 References:

- 399 Bair, E., Stillinger, T., Rittger, K. & Skiles, M. COVID-19 lockdowns show reduced pollution
400 on snow and ice in the Indus River Basin. *Proc. Natl. Acad. Sci. U. S. A.* 118, 19–21,
401 <https://doi.org/10.1073/pnas.2101174118>, 2021. Bolch, T. *et al.* Status and Change of
402 the Cryosphere in the Extended Hindu Kush Himalaya Region. in *The Hindu Kush
403 Himalaya Assessment: Mountains, Climate Change, Sustainability and People* (eds.
404 Wester, P., Mishra, A., Mukherji, A. & Shrestha, A. B.) 209–255 (Springer International
405 Publishing). doi:10.1007/978-3-319-92288-1_7 2019, 2019.
- 406 Cruz, R.V., Harasawa, H., Lal, M., Wu, S, Anokhin, Y., Punsalmaa, B., Honda, Y., Jafari, M.,
407 Li, C., and Huu Ninh, N. Climate change 2001: impacts, adaptation, and vulnerability.
408 *Choice Rev. Online* 39, 39-3433-39–3433, 2007.
- 409 Fadnavis, S. Müller R., Chakraborty T., Sabin T. P., Laakso A., Rap A., Griessbach S., Vernier
410 J-P. & Tilmes S. The role of tropical volcanic eruptions in exacerbating Indian droughts.
411 *Sci. Rep.* 11, 1–13, <https://doi.org/10.1038/s41598-021-81566-0>, 2021.
- 412 Fadnavis, S., Müller R., Kalita G, Rowlinson M., Rap A., Frank Li J-L, Gasparini B, and
413 Laakso A., The impact of recent changes in Asian anthropogenic emissions of SO₂ on
414 sulfate loading in the upper troposphere and lower stratosphere and the associated
415 radiative changes, *ACP*, 19, 9989–10008, 2019a.
- 416 Fadnavis, S., Sabin T. P., Roy C., Rowlinson M, Rap A, Vernier J-P.& E. Sioris C. E.. Elevated
417 aerosol layer over South Asia worsens the Indian droughts. *Sci. Rep.* 9, 1–12,
418 <https://doi.org/10.1038/s41598-019-46704-9>, 2019b.
- 419 Fadnavis, S., Kalita, G., Ravi Kumar, K., Gasparini, B. & Li, J. L. F. Potential impact of
420 carbonaceous aerosol on the upper troposphere and lower stratosphere (UTLS) and
421 precipitation during Asian summer monsoon in a global model simulation. *Atmos.
422 Chem.Phys.* 17, 11637–11654, <https://doi.org/10.5194/acp-17-11637-2017>, 2017.

423 Fadnavis, S., Sabin T. P, Rap A., Müller R., Kubin A. and Heinold B., The impact of COVID-
424 19 lockdown measures on the Indian summer monsoon. *Environ. Res. Lett.* 16, DOI
425 10.1088/1748-9326/ac109c, 2021.

426 Forster, P. M. *et al.* Current and future global climate impacts resulting from COVID-19.
427 *Nat.Clim. Chang.* 10, 913–919, 2020.

428 Gogoi, M. M. S. Babu S., Arun B. S., Krishna, Moorthy K., Ajay A., Ajay P., Suryavanshi A.,
429 Borgohain A., *et al.* Response of Ambient BC Concentration Across the Indian Region
430 to the Nation-Wide Lockdown: Results from the ARFINET Measurements of ISRO-
431 GBP.*Curr. Sci.* 120, 341, doi: 10.18520/cs/v120/i2/341-351, 2021.

432 Hall, D. K. MODIS / Terra Snow Cover 5-Min L2 Swath 500m. *Color. USA NASA Natl. Snow*
433 *Ice Data Cent. Distrib. Act. Arch. Cent* 5, 2006.

434 Hock, R. *et al.* Chapter 2: High Mountain Areas. IPCC Special Report on the Ocean and
435 Cryosphere in a Changing Climate. *IPCC Spec. Rep. Ocean Cryosph. a Chang. Clim.*
436 131–202, 2019.

437 Huang, W. T. K. Aerosol effects on climate, with an emphasis on the Arctic.
438 <https://doi.org/10.3929/ethz-b-000319114> 2018, 2018.

439 Hussain, A. Sarangi G.K., Pandit A., Ishaq S., Mammun N., Ahmad B., Jamil M.K., Hydropower
440 development in the Hindu Kush Himalayan region: Issues, policies and opportunities.
441 *Renew. Sustain. Energy Rev.* 107, 446–461, <https://doi.org/10.1016/j.rser.2019.03.010>,
442 2019.

443 IPCC Working Group 1, I. *et al.* IPCC, 2013: Climate Change 2013: The Physical Science
444 Basis. Contribution of Working Group I to the Fifth Assessment Report of
445 the Intergovernmental Panel on Climate Change. *Ippc AR5*, 1535, 2013.

446 Jones, C. D., et al. The climate response to emissions reductions due to COVID-19: Initial
447 results from CovidMIP. *Geophysical Research Letters*, 48, e2020GL091883.
448 <https://doi.org/10.1029/2020GL091883>, 2021.

449 Kanniah, K. D., Kamarul Zaman, N. A. F., Kaskaoutis, D. G. & Latif, M. T. COVID-19's
450 impact on the atmospheric environment in the Southeast Asia region. *Sci. Total*
451 *Environ.* 736, 139658, <https://doi.org/10.1016/j.scitotenv.2020.1396580048-9697>, 2020.

452 Krishnan, R. *et al.* Assessment of climate change over the Indian region: A report of the
453 ministry of earth sciences (MOES), government of India. Assessment of Climate Change
454 over the Indian Region: A Report of the Ministry of Earth Sciences (MoES), Government
455 of India (Springer Singapore). doi:10.1007/978-981-15-4327-2, 2020.

456 Krishnan, R., Shrestha, A., Ren, G., Rajbhandari, R., Saeed, S., & Sanjay, J. Unravelling
457 Climate Change in the Hindu Kush Himalaya: Rapid Warming in the Mountains and
458 Increasing Extremes. The Hindu Kush Himalaya Assessment (Springer Singapore).
459 doi:10.1007/978-3-319-92288-1_3, 2019.1 , 2019.

460 Laakso A. The impact of recent changes in Asian anthropogenic emissions of SO₂ on sulfate
461 loading in the upper troposphere and lower stratosphere and the associated radiative
462 changes.. *Atmos. Chem. Phys.* 1–44, <https://doi.org/10.5194/acp-19-9989-2019>, 2019a.

463 Lamarque J.-F. , Bond T. C., Eyring V., Granier C., Heil A., Klimont Z., Lee D., Liousse C.,
464 Mieville A., Owen B., Schultz M. G., Shindell D., Smith S. J., Stehfest E., Aardenne J.
465 Van, Cooper O. R., Kainuma M., Mahowald N., McConnell J. R., Naik V., Riahi K., and
466 Vuuren D. P. van, Historical (1850-2000) gridded anthropogenic and biomass burning
467 emissions of reactive gases and aerosols: Methodology and application. *Atmos. Chem.*
468 *phys.* 10, 7017–7039, <https://doi.org/10.5194/acp-10-7017-2010>, 2010.

469 Lau, W. K. M., Kim, M. K., Kim, K. M. & Lee, W. S. Enhanced surface warming and
470 accelerated snow melt in the Himalayas and Tibetan Plateau induced by absorbing
471 aerosols. *Environ. Res. Lett.* 5, doi:10.1088/1748-9326/5/2/025204, 2010.

472 Le Quéré, C. Jackson R. B., M Jones M. W., Smith A. J. P., Abernethy S. Andrew R. M. , De-
473 Gol A. J. Willi D. R., Shan Y., Canadell J. G., Friedlingstein P., Creutzig F. and Peters
474 G. P., Temporary reduction in daily global CO2 emissions during the COVID-19 forced
475 confinement. *Nat. Clim. Chang.* 10, 647–653, [https://doi.org/10.1038/s41558-020-0797-](https://doi.org/10.1038/s41558-020-0797-x)
476 [x](https://doi.org/10.1038/s41558-020-0797-x)., 2020.

477 Lee, E., Carrivick1 J. L., Quincey D. J., Cook S. J., ames1 W. H. M., &. Brown L. E.,
478 Accelerated mass loss of Himalayan glaciers since the Little Ice Age. *Sci. Rep.* 11, 1–8,
479 <https://doi.org/10.1038/s41598-021-03805-8>, 2021b.

480 Lee, S. S., Chu, J. E., Timmermann, A., Chung, E. S. & Lee, J. Y. East Asian climate response
481 to COVID-19 lockdown measures in China. *Sci. Rep.* 11, 1–9, 2021a.

482 Liu, Y. Wang Y. , Cao Y., Yang Xi, T Zhang T., Luan M., Lyu D., Hansen A. D. A., Liu B., and
483 Liu, Y., Fang, Y., Li, D., and Margulis, S. A.: How Well do Global Snow Products Characterize
484 Snow Storage in High Mountain Asia?, *Geophysical Research Letters*, 49,
485 e2022GL100082, <https://doi.org/10.1029/2022GL100082>, 2022.

486 Ma, J. Zhang T., and GUAN X., The dominant role of snow/ice Albedo feedback strengthened
487 by black carbon in the enhanced warming over the Himalayas. *J. Clim.* 32, 5883–5899,
488 <https://doi.org/10.1175/JCLI-D-18-0720.s1.2019>.

489 Martonchik, J. V., Diner, D. J., Kahn, R., Gaitley, B. & Holben, B. N. Comparison of MISR
490 and AERONET aerosol optical depths over desert sites. *Geophys. Res. Lett.* 31, 1–4,
491 <https://doi.org/10.1029/2004GL019807>, 2004.

492 Nair, V. S. Babu S. S., Moorthy K. K., Sharma A. K. , Marinoni A. & Ajai, Black carbon aerosols
493 over the Himalayas: Direct and surface albedo forcing. *Tellus, Ser. B Chem. Phys.*
494 *Meteorol.* 468 65, DOI: 10.3402/tellusb.v65i0.19738, 2013.

495 Pandey, S. K. & Vinoj, V. Surprising changes in aerosol loading over india amid covid-19
496 lockdown. *Aerosol Air Qual. Res.* 21, 1–12, <https://doi.org/10.4209/aaqr.2020.07.0466>,
497 2021.

498 Qian, Y., Flanner, M. G., Leung, L. R. & Wang, W. Sensitivity studies on the impacts of
499 Tibetan Plateau snowpack pollution on the Asian hydrological cycle and monsoon
500 climate. *Atmos. Chem. Phys.* 11, 1929–1948, doi:10.5194/acp-11-1929-2011, 2011.

501 Rogelj, J. Schaefferc M., Meinshausene M., Shindell D. T, Harec W., Klimontb Z. , Veldersh
502 G. J. M., Amannb M., and Schellnhuberr H.J., Disentangling the effects of CO2 and short
503 lived climate forcer mitigation. *Proc. Natl. Acad. Sci. U. S. A.* 111, 16325–16330,
504 <https://doi.org/10.1073/pnas.1415631111>, 2014.

505 Sabin, T., Krishnan, R., Vellore, R., Priya, P., Borgaonkar, H., Singh, B., Sagar, A. Droughts
506 and floods. *Climate Change Over the Himalayas. Assessment Of Climate Change Over*
507 *The Indian Region.* doi:10.1007/978-981-15-4327-2_11, 2020.

508 Santra, S. Verma1 S., Fujita K, Chakraborty I, Boucher O., Takemura T., Burkhardt John F.,
509 Matt F, and Sharma M., Simulations of black carbon (BC) aerosol impact over Hindu
510 Kush Himalayan sites: Validation, sources, and implications on glacier runoff. *Atmos.*
511 *Chem. Phys.* 19, 2441–2460, <https://doi.org/10.5194/acp-19-2441-2019>, 2019.

512 Sarangi, C. Qian Y., Rittger K., Bormann K.J., Liu Y., Wang H., Wan H., Lin G., and. Painter
513 T.H., Impact of light-absorbing particles on snow albedo darkening and associated
514 radiative forcing over high-mountain Asia: high-resolution WRF-Chem modeling and
515 new satellite observations. *Atmos. Chem. Phys.* 19, 7105–7128,
516 <https://doi.org/10.5194/acp-19-7105-2019>, 2019.

517 Sarangi, C., Qian, Y., Rittger, K., Ruby Leung, L., Chand, D., Bormann, K. J., and Painter, T.
518 H.: Dust dominates high-altitude snow darkening and melt over high-mountain Asia,
519 Nature Climate Change, 10, 1045-1051, 10.1038/s41558-020-00909-3, 2020.

520 Schultz, M. G., Stadtler S., Schröder S., Taraborrelli D., Franco B., Krefting J, Henrot A. et al.,
521 The chemistry-climate model ECHAM6.3-HAM2.3-MOZ1.0. *Geosci. Model Dev.* 11,
522 1695–1723, <https://doi.org/10.5194/gmd-11-1695-2018>, 2018.

523 Shafeeque, M. Arshad A., A Elbeltagi A., Sarwar A., Pham Q. B., S Khan S. N., I Dilawar A.
524 & Al-Ansari N., Understanding temporary reduction in atmospheric pollution and its
525 impacts on coastal aquatic system during COVID-19 lockdown: a case study of South
526 Asia. *Geomatics, Nat. Hazards Risk* 12, 560–580,
527 <https://doi.org/10.1080/19475705.2021.1885503>, 2021.

528 Srivastava, A. K., Bhojar P.D., K 499 anawade V. P., Devara P.C. S., Thomas A., Soni V.K.,
529 Improved air quality during COVID-19 at an urban megacity over the Indo-Gangetic
530 Basin: From stringent to relaxed lockdown phases. *Urban Clim.* 36, 100791,
531 <https://doi.org/10.1016/j.uclim.2021.100791>, 2021.

532 Stevens, B., Giorgetta M., Esch M., Mauritsen T., Crueger T., Rast S., Salzmann M., Schmidt
533 H., Bader J., Block K., Brokopf R., Fast I., Kinne S., Kornblueh L., Lohmann U., Pincus
534 R., Reichler T., Roeckner E. Atmospheric component of the MPI-M earth system model:
535 ECHAM6. *J. Adv. Model. Earth Syst.* 5, 146–172, <https://doi.org/10.1002/jame.20015>,
536 2013.

537 Stier, P., Feichter J., Kinne S., Kloster S., Vignati E., Wilson J., Ganzeveld L., Tegen I., Werner
538 M., Balkanski Y. Schulz M., Boucher O., Minikin A., and Petzold A., The aerosol-climate
539 model ECHAM5-HAM. *Atmos. Chem. Phys.* 5, 1125–1156, [https://doi.org/10.5194/acp-](https://doi.org/10.5194/acp-5-1125-2005)
540 [5-1125-2005](https://doi.org/10.5194/acp-5-1125-2005), 2005.

541 Tegen, I., Neubauer D., Ferrachat S., Siegenthaler-Le Drian C, Bey, I., Schutgens N., Stier P.,
542 Watson-Parris D., et al., The global aerosol-climate model echam6.3-ham2.3 -Part 1:
543 Aerosol evaluation. *Geosci. Model Dev.* 12, 1643–1677, [https://doi.org/10.5194/gmd-12-](https://doi.org/10.5194/gmd-12-1643-2019)
544 1643-2019, 2019.

545 Textor , Schulz M, Guibert S., Kinne S., Balkanski Y., Bauer S., Berntsen T., Berglen T.,
546 Boucher O., Chin M., Dentener F, Diehl T., Easter R., Feichter H., Fillmore D., Ghan
547 S., Ginoux P., Gong S., Grini A., Hendricks J. , Horowitz L., Huang P., Isaksen I., Iversen
548 I, Kloster S., Koch D., Kirkevåg A., Kristjansson J. E., Krol M., Lauer A., Lamarque J.
549 F., Liu X., Montanaro V., Myhre G., Penner J., Pitari G., Reddy S., Seland Ø., Stier P.,
550 Takemura T., and Tie X., Analysis and quantification of the diversities of aerosol life
551 cycles within AeroCom. *Atmos. Chem. Phys.* 6, 1777–1813, [https://doi.org/10.5194/acp-](https://doi.org/10.5194/acp-6-1777-2006)
552 6-1777-2006, 2006.

553 Thind, P. S., Chandel, K. K., Sharma, S. K., Mandal, T. K. & John, S. Light-absorbing
554 impurities in snow of the Indian Western Himalayas: impact on snow albedo, radiative
555 forcing, and enhanced melting. *Environ. Sci. Pollut. Res.* 26, 7566–7578,
556 <https://doi.org/10.1007/s11356-019-04183-5>, 2019.

557 Tiwari, S., Kar, S. C. & Bhatla, R. Snowfall and Snowmelt Variability over Himalayan Region
558 in Inter-annual Timescale. *Aquat. Procedia* 4, 942–949,doi:
559 10.1016/j.aqpro.2015.02.118, 2015.

560 Usha, K. H., Nair, V. S. & Babu, S. S. Effect of aerosol-induced snow darkening on the direct
561 radiative effect of aerosols over the Himalayan region. *Environ. Res. Lett.* 16,
562 <https://doi.org/10.1088/1748-9326/abf190>, 2021.

563 Wester P., Mishra A., Mukherji A., S. A. B. The Hindu Kush Himalaya Assessment—
564 Mountains, Climate Change, Sustainability and People. Springer Nature Switzerland AG,
565 Cham. doi:<https://doi.org/10.1007/978-3-319-92288-1>, 2019.

566 Wood, L. R. Neumann K., Nicholson K.N., Bird B.W., Dowling C. B. and Sharma S.. Melting
567 Himalayan Glaciers Threaten Domestic Water Resources in the Mount Everest Region,
568 Nepal. *Front. Earth Sci.* 8, 1–8, <https://doi.org/10.3389/feart.2020.00128>, 2020.

569 Zhang, K. O'Donnell D., Kazil J., Stier P., Kinne S., Lohmann U., Ferrachat S., Croft B., Quaas
570 J, Wan H., Rast S., and Feichter J., The global aerosol-climate model ECHAMHAM,
571 version 2: Sensitivity to improvements in process representations. *Atmos. Chem.Phys.*
572 12, 8911–8949, <https://doi.org/10.5194/acp-12-8911-2012>, 2012.

573 Zheng M., Impacts of COVID-19 on Black Carbon in Two Representative Regions in China:
574 Insights Based on Online Measurement in Beijing and Tibet. *Geophys. Res. Lett.* 48, 1–
575 11, [10.1029/2021GL092770](https://doi.org/10.1029/2021GL092770), 2021.

576

577 **Acknowledgments**

578 The authors thank the staff of the High Power Computing Centre (HPC) in IITM, Pune, India,
579 for providing computer resources and the team members of MODIS for providing data. We
580 thank Sabur F. Abdullaev and Brent Holben for their efforts in establishing and maintaining
581 Dushanbe and Lahore AERONET sites respectively. Work done in the manuscript is not
582 supported by any funding agency.

583 **Funding information**

584 The manuscript is not funded.

585 **Author Contributions**

586 S.F. initiated the idea of the study. S.F. and B. H. performed model simulations. A.R. and A.
587 K. prepared Google based emission inventory. T.P.S., A.A., R.M. performed data analysis and
588 contributed in overall design. All authors contributed to discussions of the results and the
589 writing of the manuscript.

590 **Data and code availability**

591 The ECHAM-HAMMOZ model source code and all required input data are available to the
592 scientific community according to the HAMMOZ Software License Agreement through the
593 project website: <https://redmine.hammoz.ethz.ch/projects/hammoz>. The data that support the
594 findings of this study are openly available in zenodo at <http://doi.org/.../zenodo...>

595

596 **Competing Interests:** Two of the (co-)authors are members of the editorial board of
597 Atmospheric Chemistry and Physics.